NASA CONTRACTOR
REPORT

NASA CR-1494
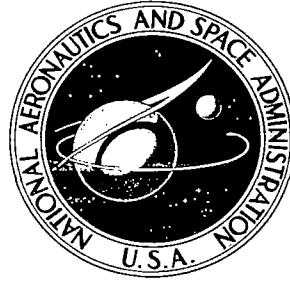
THEORETICAL STUDY OF
DUCTED FAN PERFORMANCE

by Michael R. Mendenhall and Selden B. Spangler

NATIONAL AERONAUTICS AND SPACE ADMINISTRATION • WASHINGTON, D. C. • JANUARY 1970

NASA CR-1494

THEORETICAL STUDY OF

DUCTED FAN PERFORMANCE

By Michael R. Mendenhall and Selden B. Spangler

Distribution of this report is provided in the interest of information exchange. Responsibility for the contents resides in the author or organization that prepared it.

Issued by Originator as NEAR TR 15

TABLE OF CONTENTS

THEORETICAL STUDY OF

DUCTED FAN PERFORMANCE

By Michael R. Mendenhall and Selden B. Spangler
Nielsen Engineering & Research, Inc.

SUMMARY

Analysis and programming work have been conducted to provide an improved capability to an existing computer program developed previously by the authors for predicting the performance of a ducted fan in a uniform axial flow. The capabilities have been added for modeling the centerbody, providing nonlinear blade lift characteristics, calculating performance at very low advance ratios, computing duct surface pressure distributions, and computing performance at angle of attack. The additional analysis is described in this report. The resulting computer program is described in detail in a second document, reference 1, which is essentially a user's manual.

The computer program considers a prescribed ducted fan operating at a given advance ratio in a uniform flow at angle of attack. The ducted fan is described by the duct chord-to-diameter ratio, duct camber and thickness distribution, centerbody shape, axial location of the fan, number of fan blades, and the radial variation of fan blade chord, pitch angle and thickness-to-chord ratio. The computer program solves for the blade loading, fan inflow profiles, forces and moments on the ducted fan, and chordwise pressure distributions on the duct at specified azimuth angles. Comparisons with data for two ducted fans are presented in the user's manual which indicate generally good agreement on all performance parameters except pitching moment.

INTRODUCTION

This report is one of two documents prepared under Contract NAS2-4953 for the Ames Research Center, NASA. The work under this contract is concerned with development of methods for predicting the aerodynamic performance of ducted fans in uniform flow. This report describes the analysis performed under the contract. The second document, reference 1, is a user's manual for the computer program developed to predict ducted fan performance.

The authors and their associates have done a considerable amount of prior work on ducted fan analysis (refs. 2-8). The final task of that work involved the preparation of a computer program for calculating the aerodynamic characteristics of a ducted fan in a uniform, axial flow (ref. 8). The purpose of the present investigation is to make certain improvements and additions to the computer program of reference 8. The additional analysis required to make these improvements is reported herein. Since the improved computer program described in reference 1 is based on much of the earlier analysis as well as the analysis reported herein, the manual (ref. 1) contains appropriate references to equations, methods, and results of references 2 through 8 as well as this document.

Considerable familiarity with the previous ducted fan work is assumed in the technical discussion of this report. In order to introduce the work reported herein and place it in perspective, the remainder of this section is devoted to a brief description of the earlier work and its relation to the work of other investigators. In addition, a brief description of the entire flow model is presented in the following section. Only isolated ducted fans are considered; that is, no duct-duct or duct-airframe interference effects are discussed.[1]

The initial work by the authors and their associates (refs. 2 and 3) was concerned with the forces and moments on a ducted fan as they might affect the stability characteristics of an aircraft configuration. The desired quantities were the variation of forces and moments on the ducted fan with angle of attack and pitching angular velocity. In order to obtain the stability derivatives and nonlinear force behavior, a relatively simple potential flow model was used, but no limitations were placed on angle of attack, thrust, or duct chord-to-diameter ratio. The duct was permitted to have thickness and camber, but the details of the fan, centerbody, and strut system were ignored. These were replaced by a uniformly loaded actuator disk. The fan wake was assumed to be a cylinder of constant diameter equal to the duct trailing-edge diameter and coaxial with the duct centerline. This approach yielded the desired static and damping derivatives in pitch and nonlinear force and moment

---

[1]Duct-duct interference is considered in references 3 and 7, and duct-hull interference is considered in references 4 and 5, where some indication of the importance of interference effects can be obtained.

2

variations with angle of attack. Some examples of the agreement with data are given in reference 6. In contrast, the work of Therm, as summarized in references 9 and 10, and the work done at the Naval Ship Research and Development Center by Morgan (ref. 11), Chaplin (ref. 12), and Caster (ref. 13) were more concerned with the details of the flow through the fan and in the fan wake. Because of the increased complexity and difficulty of considering flow details in the fan and wake, the work just cited was limited to zero (or small, in some cases) angles of attack.

The work of reference 3 resulted in a method for predicting force and moment coefficients on the ducted fan if the fan thrust or fan wake velocity was known. The work reported in reference 7 removed the necessity for knowing or assuming fan thrust. For axial flow, the fan blade performance within the duct was related to the local inflow through blade element theory. The blade loading was permitted to change radially to correspond to variable inlet flow velocities and blade characteristics. Concentric fan wake vortex cylinders, whose strengths were related to the radial variation of blade loading, were considered to be shed from the fan. Previous methods were then used to obtain the resulting duct-bound vorticity and overall performance in axial flow. As a result of this work, a computer program was prepared (ref. 8), which would compute the performance of a given fan-duct combination in axial flow at a prescribed advance ratio.

In the work of references 2 through 8, a number of analyses and/or approaches were developed which were not incorporated into the program of reference 8 but which could represent significant improvements in the capability and utility of the program. The purpose of the present investigation is to perform the necessary analysis and incorporate the improvements in the program, and document the changes. The specific areas considered are the following:

(1) Inclusion of a centerbody model.
(2) Removal of an arbitrary limitation on low advance ratios.
(3) Incorporation of nonlinear blade characteristics.
(4) Incorporation of a duct pressure distribution calculation.
(5) Incorporation of an angle of attack capability in the calculation.

3

The analysis for these improvements, to the extent that it is not described in the earlier work, is described in this report. The modified computer program is documented in reference 1.

This introduction has referred briefly to the work of other investigators who have examined various facets of ducted fan performance and design. A comprehensive survey in this area was presented at the Seventh ONR Symposium on Naval Hydrodynamics given at Rome, Italy in August 1968. The specific papers are references 14 and 15. These papers will appear in a bound edition of the Conference proceedings to be published by ONR in 1970.

SYMBOLS

A   area of duct at the exit plane, $\pi D^2/4$

A_n Fourier series coefficients for the radial velocity induced on the reference cylinder by all the internal vortex cylinders

A_n^* Fourier series coefficients for the axial velocity induced on the reference cylinder by all the internal vortex cylinders

A_p fan disk area, $\pi (R_p^2 - R_{CB}^{\ 2})$

a   half of the distance between the point source and point sink of the Rankine centerbody

B_n Fourier series coefficients for the radial velocity induced on the reference cylinder by the outer trailing vortex cylinder

B_n^* Fourier series coefficients for the axial velocity induced on the reference cylinder by the outer trailing vortex cylinder

b   blade chord

C_{CB} correction factor for centerbody-induced velocities, eq. (3)

C_J correction factor for duct-thickness-induced velocities, eq. (1)

C_M pitching-moment coefficient, M/RAq

C_N normal-force coefficient, N/Aq

C_n Glauert series coefficients for γ_D, eq. (64)

C_p pressure coefficient, $(p - p_\infty)/q$, eq. (68)

C_T thrust coefficient, T/Aq

c chord length of duct

c_ℓ lift coefficient for fan blade section

c_{ℓ_α} lift curve slope for fan blade section

$c_{\ell_{max}}$ maximum section lift coefficient

c_n Glauert series coefficients for γ_α, eq. (31)

D diameter of duct at the exit plane

D_n Fourier series coefficients for the radial velocity induced on the reference cylinder by the centerbody

D_n^* Fourier series coefficients for the axial velocity induced on the reference cylinder by the centerbody

D_p fan diameter

E_n Fourier series coefficients for the radial velocity induced on the reference cylinder by γ, γ_w, and the centerbody, eq. (33)

E_n^* Fourier series coefficients for the axial velocity induced on the reference cylinder by γ_D, γ, γ_w, and the centerbody, eq. (45)

E_n' Fourier series coefficients for the radial velocity induced on the reference cylinder by γ_D, γ, γ_w, and the centerbody, eq. (61)

F_n Fourier series coefficients for the radial velocity induced on the reference cylinder by the duct-bound vorticity

F_n^* Fourier series coefficients for the axial velocity induced on the reference cylinder by the duct-bound vorticity

$F(x)$ scaling factor, eq. (65)

G_n integrals defined by eq. (23)

G_n^* Fourier series coefficients for the axial velocity induced on the reference cylinder by the γ_α vorticity, eq. (49)

H_n Fourier series coefficients for the radial velocity induced on the reference cylinder by the trailing vortex filaments associated with γ_α

h   fan blade thickness, or maximum radius of Rankine body

I_n integrals defined by eq. (10) or (24)

J   fan advance ratio, V/nD_p

J'   advance ratio parameter, $V/\omega R$

$\overline{J}$ effective fan advance ratio, $V \cos \alpha / nD_p$

$\overline{J}'$ effective advance ratio parameter, $J' \cos \alpha$

ℓ_{CB} length of centerbody

ℓ_s length of line source

M   pitching moment

M_n coefficients of polynomial describing line source, eq. (5) and (20)

m   source strength, eq. (5)

m_s sink strength, eq. (8)

N   number of fan blades or normal force

n   fan rotational speed, rev/sec

p_∞ free-stream static pressure

q   free-stream dynamic pressure, $\rho V^2/2$

R   radius of duct at the exit plane, D/2

R_{CB} radius of fan root (nominally same as centerbody radius at fan station)

Re_c Reynolds number based on airfoil chord length

R_p radius of fan tip

r   local radius measured from duct centerline

r_{CB} local centerbody radius, eq. (7)

T   thrust force

6

u	induced axial velocity
u_{CB}	axial velocity induced by centerbody singularity distribution
u_{q_d}	axial velocity induced by duct thickness distribution
u_s	duct surface velocity
u_γ	axial velocity induced by the vortex cylinder trailing from the duct trailing edge
u_{γ_w}	sum of the axial velocities induced by all internal vortex cylinders trailing from the fan
u_{γ_D}	axial velocity induced by duct-bound vorticity, γ_D
u_{γ_α}	axial velocity induced by duct-bound vorticity, γ_α
V	free-stream velocity
$\bar{V}$	effective free-stream velocity, $V \cos \alpha$
v_{CB}	radial velocity induced by centerbody singularity distribution
v_γ	radial velocity induced by vortex cylinder trailing from the trailing edge of duct
v_{γ_t}	radial velocity induced by the trailing vortex filaments associated with γ_α, eq. (40)
v_{γ_w}	sum of the radial velocities induced by all internal vortex cylinders trailing from the fan
v_{γ_D}	radial velocity induced by duct-bound vorticity, γ_D
x	axial distance from leading edge of duct
x_{CB}	location of centerbody nose in duct coordinate system
x_m	location of sink in centerbody model
x_s	axial distance measured aft from the duct midchord
z	number of equal area elements making up fan disk area
α	free-stream angle of attack
α_o	angle of attack for zero lift

7

γ strength of outer trailing vortex cylinder

γ_w strength of wth inner trailing vortex cylinder

γ_D axially symmetric component of duct-bound vorticity, eq. (64)

γ_α duct-bound vorticity component due to angle of attack, eq. (31)

Δp rise in static and total pressure across actuator disk

Δp_z rise in static pressure in outermost annulus of actuator disk

θ transformed axial distance, $x = 1/2 (1 - c \cos \theta)$

ψ stream function

ρ free-stream density

ϕ azimuthal angle, see fig. 1(b)

ξ axial coordinate in centerbody coordinate system

ζ axial coordinate in Rankine body

ω fan rotational speed, rad/sec

Subscripts

CB   due to centerbody

D   for the duct in the presence of the fan

P   for the fan shrouded by the duct

γ due to outer vortex cylinder trailing from duct trailing edge

γ_D due to duct-bound vorticity, γ_D

γ_w due to all internal vortex cylinders trailing from fan

γ_α due to duct-bound vorticity, γ_α

DESCRIPTION OF FLOW MODEL

A brief description of the flow model and general approach to the calculation of ducted fan performance is given in this section in order to relate the analysis of the following sections to the overall method of approach. The model considers a ducted fan in a uniform flow at an

8

angle of attack which is not necessarily small. No interference with other ducted fans or airframe components is considered. The flow is assumed to be inviscid. Potential flow methods are used, and advantage is taken of the fact that solutions properly satisfying the boundary conditions may be superimposed to obtain the overall model.

The two basic solutions used in the method are illustrated in figure 1. They are an axial flow solution for the fan-duct-centerbody combination and an angle of attack solution for the duct. In the axial flow solution, the flow interaction between the fan, duct with thickness and camber, and centerbody is considered. The fan is specified by the number of blades and the variation with radius of blade chord, pitch angle, and thickness. The blade loading at a given radius is obtained from the known (or assumed) axial inflow, the blade speed, and section characteristics. This calculation, performed at a number of radial stations, yields the radial variation of blade loading. To the extent that the loading (the blade bound vorticity) varies between one radial station and the next, a vortex cylinder is assumed to be shed between the stations, whose strength is the difference in bound vorticity, and is noted γ_w in figure 1(a). Thus, the fan wake consists of a series of concentric vortex cylinders, with the outermost cylinder assumed to be shed from the tip, to lie along the inner duct surface and to trail from the duct trailing edge.

The duct may have camber and thickness. Source rings are used to represent the thickness distribution, and the induced camber due to the source rings is taken into account. A reference cylinder is defined for purposes of satisfying the flow tangency condition on the duct. This cylinder has a radius R equal to the duct trailing-edge radius. Although the flow is assumed tangent to the local camberline slope, the velocities are actually computed at a radius of R for purposes of enforcing the tangency condition.

The centerbody is assumed to operate in a uniform flow equal to the inflow velocity to the fan near its hub. A simple source-sink distribution is used to represent the centerbody configuration.

The calculation proceeds as follows. The fan-duct-centerbody configuration is assumed known, and the advance ratio is selected. A uniform inflow to the fan is assumed initially, and the fan wake vortex cylinder

strengths are determined (γ and γ_w) from the local blade element calculations. The centerbody source-sink representation is calculated. Then the radial and axial velocity distributions along the duct reference cylinder induced by the centerbody and wake cylinders are computed and Fourier analyzed. A ring vortex distribution, γ_D, which is expressed as a Glauert series, is placed on the duct. The unknown series coefficients of γ_D are computed by requiring that the velocity distribution induced by γ_D, expressed in Fourier series form, combine with the velocity distributions induced by the centerbody, wake cylinders, and free stream to cause the net velocity to be tangent to the camberline along the duct chord. Once this γ_D distribution is known, the blade inflow due to all causes can be calculated, compared with the assumed distribution, and a new distribution used in an iterative solution to converge on a set of consistent singularity distributions.

The second solution is that for a thin cylindrical duct at angle of attack, as illustrated in figure 1(b). The crossflow component of the free stream, V sin α, provides a radial velocity through the duct which varies with cos ϕ. A chordwise distribution of vortex rings whose strength γ_α varies with cos ϕ, together with the necessary trailing vortex filaments, is placed on the duct so that the induced radial velocity just cancels the V sin α cos ϕ component.

The V sin α component of the free stream has some effect on the centerbody and fan as well as on the duct. These effects were ignored, primarily for the following reasons. First, the effects of nonuniform circumferential loading on the fan due to angle of attack become extremely complicated to analyze (see ref. 7) and the effects do not appear sufficiently important to justify the additional complexity of the analysis. Second, the duct tends to align the flow to minimize crossflow effects on the fan and centerbody.

The singularity distributions for the two solutions are superimposed to obtain the complete solution and the forces, moments, and pressure distributions are obtained. The duct force distribution is determined from the action of a velocity on an element of bound singularity. Using the proper combinations of velocity and vorticity, the elemental force distribution can be integrated to obtain duct forces and moments. The fan thrust is added to the duct thrust to obtain total thrust.

10

Pressure distributions on the duct are obtained from the duct surface
velocity distribution using the Bernoulli equation.

This description is brief, but covers the essence of the approach.
For further details, references 1, 3, 6, and 7 can be consulted.

NONLINEAR BLADE LIFT CURVE

The computer program of reference 8 was developed using linear
blade section lift characteristics. The fan annulus is divided into a
number of annuli of equal area in each of which the blade performance is
assumed to be uniform. The blade loading is determined by computing the
axial inflow velocity, combining this with the blade rotational velocity
to get the velocity relative to the blade, and comparing the direction
of this relative velocity vector with the angle of zero lift of the
blade to get the angle of attack. The angle of attack is then used with
a lift curve slope of 2π to obtain the section-lift coefficient. Thus,
the program of reference 8 is incapable of including any nonlinear lift
effects due to separation and stall of the blade.

The first step in the task to incorporate nonlinear lift effects
was to investigate the aerodynamic characteristics of real blade sections.
Figure 2(a) is a plot of section-lift coefficient versus flow incidence
angle measured from the angle of zero lift $(\alpha - \alpha_o)$ for a number of
airfoil sections of varying thickness and camber. The data were
obtained from reference 16. The angle of attack at which the curves
depart from the theoretical curve $(c_{\ell_\alpha} = 2\pi)$ depends on both camber and
thickness, with the latter being generally the largest and most consis-
tent effect. The "width of the $c_{\ell_{max}}$ " region also varies considerably;
some sections exhibit a very sharp drop in lift once stall occurs, and
some sections exhibit a nearly constant lift coefficient for a considerable
range of α. On the basis of these characteristics, it was decided that
the nonlinear representation most consistent with the use of blade
performance in the program is that illustrated in the following sketch:

11
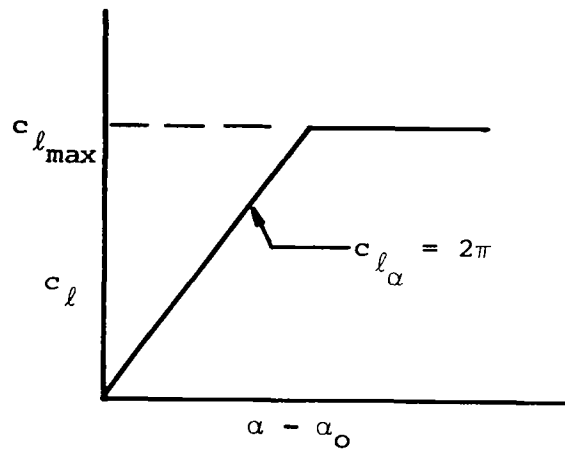
The lift curve is assumed linear up to the value of $\alpha - \alpha_o$ given
by $c_{\ell_{max}}$ and $c_{\ell_\alpha} = 2\pi$. Beyond this angle the lift coefficient
is assumed constant and equal to $c_{\ell_{max}}$. Since thickness effects are
the predominant factor in determining $c_{\ell_{max}}$, the $c_{\ell_{max}}$ values used
in the computer program are assumed to be functions only of blade thickness-
to chord ratio. Figure 2(b) shows the values of $c_{\ell_{max}}$ versus h/b
that are used in the computer program.

CORRECTION FOR LOW ADVANCE RATIO

In the analysis and computer program of references 7 and 8,
respectively, the source-sink distribution describing the duct thickness
was assumed to be in a uniform free stream V. This assumption is good
when the axial velocity induced by the bound and trailing vorticity,
γ_D and γ, is small in comparison with the free-stream velocity. At
very low advance ratios the velocity induced by the vorticity can become
large with respect to the free stream. Thus, a significant error occurs
in the computed source strength and in the source-induced velocities.
A correction was made in the following manner.

If we assume that the source distribution describing the duct
thickness is operating in an effective free stream which is made up of
the actual free stream V and the velocity induced by the bound and
trailing vorticity, the source strength should be increased by a factor
equal to the effective velocity divided by the actual free-stream

12

velocity. Since the source-induced velocity is directly proportional to
the source strength, the source-induced velocity should be increased by
the same factor. Thus, defining the correction factor to be C_J, we
have the following relations.

$$C_J = 1 + \frac{u_{\gamma_D}}{\overline{V}} + \frac{u_{\gamma}}{\overline{V}} \tag{1}$$

$$\left(\frac{u_{q_D}}{\overline{V}}\right)_{J\approx0} = \left(\frac{u_{q_D}}{\overline{V}}\right)_{J\gg0} \times C_J \tag{2}$$

The induced velocities u_{γ_D} and u_{γ} vary somewhat with distance
along the chord. The possibility of using average values of these
velocities was examined, and it was determined that sufficient accuracy
is obtained by using the values calculated at the fan station on the
duct reference cylinder. Consequently, this approach is used in the
program. The velocity u_{γ_D} induced by γ_D is computed using
equation (A-9) of reference 7, and u_{γ} is computed using equation (A-10)
of the same reference. Equation (1) does not include the effect of the
centerbody because, as is discussed in a following section, the axial
velocity induced by the centerbody is small compared with the free
stream. The axial velocity induced by all the internal vortex cylinders
does not appear in equation (1), because this velocity is zero at the
axial station at which the correction is made (the leading edges of the
cylinders).

A similar type of correction must be applied to the source distri-
bution describing the centerbody. Again, using average velocities to
compute the correction factor, and computing these velocities at the
propeller station on the axis of the duct, we get the following correc-
tion factor

$$C_{CB} = 1 + \frac{u_{\gamma_D}}{\overline{V}} + \frac{u_{\gamma}}{\overline{V}} + \frac{1}{2} \sum_{w=1}^{z-1} \frac{\gamma_w}{\overline{V}} \tag{3}$$

This equation is analogous to equation (A-12) of reference 7.

Therefore, the velocities induced by the centerbody are

$$\left(\frac{u_{CB}}{\bar{v}}\right)_{J\approx 0} = \left(\frac{u_{CB}}{\bar{v}}\right)_{J\gg 0} \times c_{CB}$$

$$\left(\frac{v_{CB}}{\bar{v}}\right)_{J\approx 0} = \left(\frac{v_{CB}}{\bar{v}}\right)_{J\gg 0} \times c_{CB}$$

(4)

CENTERBODY FLOW MODEL

The program of reference 8 was directed toward low-pressure-ratio ducted fans, such as that used on the Bell X-22A aircraft, which have small centerbodies. As a result, the centerbody has little influence on the flow through the fan, and its blockage effect was not included in the flow model of reference 8. The centerbody presence was considered, however, by requiring that the fan hub radius be that of the centerbody and the area inside this radius be unloaded. For higher pressure ratio fans, this approximation is no longer adequate, because the centerbodies tend to be large compared to the fan tip radius. Consequently, it was necessary to develop a centerbody model appropriate to higher pressure ratio fans now under consideration. The model is for axial flow and allows the calculation of the induced axial and radial velocities at any field point outside the centerbody.

The centerbody typically is a body of revolution having a rounded nose, a maximum diameter somewhere near the fan station, and a tapered after section with either a rounded or pointed tail. Test data examined under some earlier work done for the Ames Research Center, NASA, (ref. 6) indicated that flow separation probably occurs on the after (contracting) portion of the centerbody. Consequently, it was felt that the greatest accuracy in modeling the centerbody shape should occur over the forward portion, and less accuracy could be accepted in modeling the aft portion.

The centerbody model most consistent with the singularity distribution of the remainder of the ducted fan model is a source-sink distribution along the duct axis. Four approaches were considered as follows:

14

(1) A line source, whose strength distribution is approximated using slender-body theory with local body coordinates, and a point sink.

(2) A Rankine body (point source and point sink).

(3) A line source and point sink whose strengths are computed using arbitrarily selected body coordinates.

(4) A distribution of discrete sources whose strengths are determined using the body slopes.

In the first approach, the source strength is determined by considering only that source element at the axial station of interest to contribute to the velocity at the body surface, whereas in the other three approaches, all source elements contribute to the velocity at the point of interest on the body. For the line sources, power series were used to describe the strength variation with length. The theory for each of these approaches was developed and programmed, and comparisons were made for several centerbody shapes. The quantities examined were the body fit, the induced velocities at the fan station and the induced velocities on the duct reference cylinder. Of the four approaches, the two using a line source and point sink were found to give generally poor body fits, although with a number of trials using different arrangements of control points on the body surface, a fair shape fit to the forward part of the body could be obtained. Consequently, these two were judged unsuitable for use in the program. The approach using the body slopes was found to give good shape fits although again a number of trials were necessary. However, a large number of sources is required (20 to 30), and a large number of body slopes must be computed as input information. The Rankine model is simple to use and because of its characteristic shape gives good fits to relatively blunt centerbodies but not to slender, pointed centerbodies.

As a result of the investigation on centerbodies, the Rankine body model was selected for use with the program. This selection was prompted by three main factors: the generally blunt shapes of advanced engine centerbodies which are adequately fit by the Rankine shape, the simplicity of use of the Rankine model, and the fact that the centerbody-induced velocities generally are small compared to other velocities existing at the fan station and on the duct reference cylinder. In order to document the results of the investigation, the theory for the various approaches (except the fourth) are presented in the sections that follow, together with some comparisons of computed results.

Slender-Body Line Source Model

Reference 4 contains an approximate method for describing a submarine hull in a uniform axial flow using a point source near the nose and a line sink near the tail. This approach was used to construct a line source-point sink centerbody model wherein the source strength is calculated using slender-body theory. The geometry is shown in the following sketch:
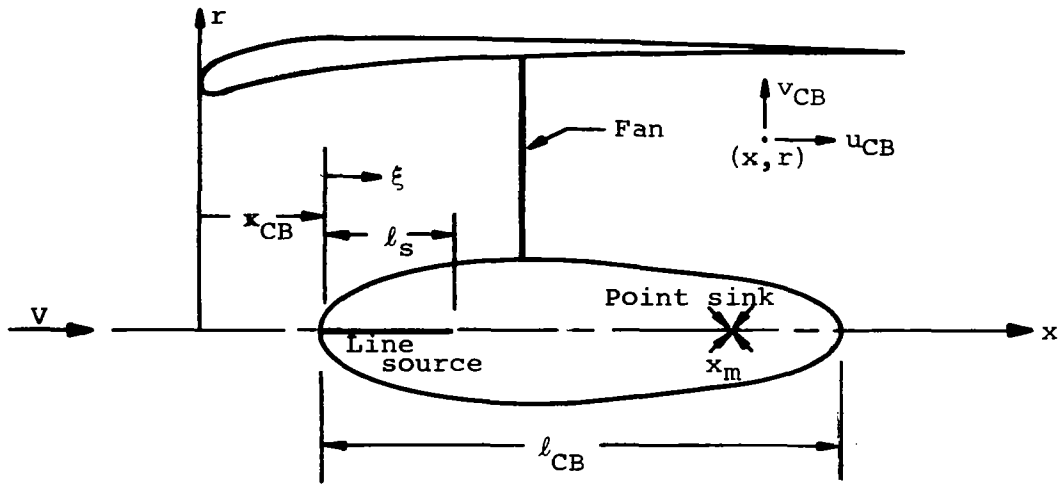
The strength distribution of the source m is represented by a third-order polynomial in distance ξ' along the source length, where $\xi' = \xi/\ell_{CB}$.[2]

$$\frac{2m}{V\ell_{CB}} = M_1\xi' + M_2\xi'^2 + M_3\xi'^3 \qquad (5)$$

One can also relate the local slope of the centerbody $dr/d\xi$ to the local source strength (at the same ξ station) through slender-body theory. Thus,

$$m = \frac{V}{2\pi}\frac{d(\pi r^2_{CB})}{d\xi} \qquad (6)$$

---

[2]The prime in the following analysis denotes a length quantity non-dimensionalized by ℓ_{CB}.

These two relations can then be combined to yield an expression for the differential of r^2_{CB} in terms of the polynomial of equation (5), which can then be integrated to obtain the following expression.

$$\frac{r^2_{CB}}{\ell^2_{CB}} = \frac{M_1 \xi'^2}{2} + \frac{M_2 \xi'^3}{3} + \frac{M_3 \xi'^4}{4} \tag{7}$$

In order to obtain the three coefficients of equation (7), it is necessary to specify the centerbody radius at three axial stations and solve the three linear simultaneous equations which result.

The three-dimensional point sink is located an arbitrary distance aft of the centerbody nose such that the centerbody has approximately the correct length. Its strength is equal and opposite to the integral of the source strength over the source length. Thus, a zero net source strength is obtained which yields a closed centerbody. The sink strength m_s is given by

$$-\frac{2m_s}{V \ell^2_{CB}} = \frac{M_1}{2} (\ell'_s)^2 + \frac{M_2}{3} (\ell'_s)^3 + \frac{M_3}{4} (\ell'_s)^4 \tag{8}$$

In this approach, the shape fits for the forward and aft portion of the centerbody are computed independently of each other. The forward part of the centerbody shape (over the length of the line source) is obtained from equation (7) using the M_n coefficients calculated by use of the three selected centerbody fit points. The aft portion of the body is given by the solution for a point sink in a uniform flow, as given for instance in reference 4.

The velocity at a field point is given by superposition of the velocities induced by each singularity distribution. Expressions for the induced velocities in the form of integrals containing m are available in reference 17. The final velocity equations are as follows.

The axial velocity induced at a point (x',r') by the line source is

$$\frac{u(x',r')}{V} = \frac{M_1}{4} \left[(x' - x'_{CB}) I_1 - I_2 \right] + \frac{M_2}{4} \left[(x' - x'_{CB}) I_2 - I_3 \right]$$

$$+ \frac{M_3}{4} \left[(x' - x'_{CB}) I_3 - I_4 \right] \tag{9}$$

17

where

$$I_n = \int_0^{\ell'_s} \frac{(\xi')^n \, d\xi'}{\left[(x' - x'_{CB} - \xi')^2 + (r')^2\right]^{3/2}} \tag{10}$$

The radial velocity induced by the line source is

$$\frac{v(x',r')}{V} = \frac{M_1 r'}{4} I_1 + \frac{M_2 r'}{4} I_2 + \frac{M_3 r'}{4} I_3 \tag{11}$$

Using equation (8), the axial velocity induced at the point (x',r') by the point sink at x_m is

$$\frac{u(x',r')}{V} = \left(\frac{m_s}{2V\ell^2_{CB}}\right) \frac{x' - x'_m}{\left[(x' - x'_m)^2 + (r')^2\right]^{3/2}} \tag{12}$$

and the radial velocity is

$$\frac{v(x',r')}{V} = \left(\frac{m_s}{2V\ell^2_{CB}}\right) \frac{r'}{\left[(x' - x'_m)^2 + (r')^2\right]^{3/2}} \tag{13}$$

At a field point (x',r') the induced axial velocity is the sum of equation (9) and (12), and the induced radial velocity is the sum of equations (11) and (13).

Rankine Body

The most simple three-dimensional centerbody model is a point source and a point sink as shown in the following sketch:
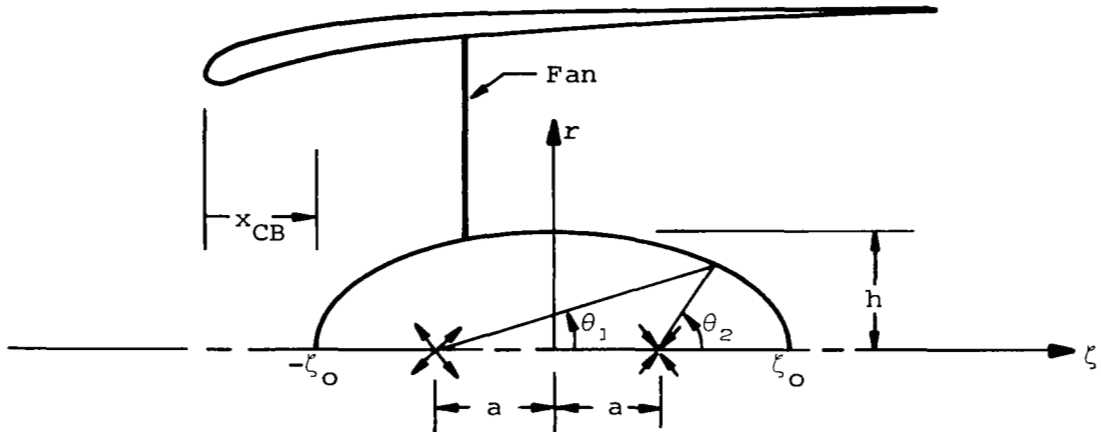
This body is nearly an ellipsoid and is usually called a Rankine body. Due to the simplicity of the model, only the maximum radius and the total length can be varied.

The equations for the Rankine body are well documented, but they will be presented for convenience. The location of the source and sink for a body of given dimensions (ζ_o, h) is found from the following equation, where the symbols are defined in the above sketch.

$$h^2 \sqrt{a^2 + h^2} = \frac{(\zeta_o^2 - a^2)^2}{\zeta_o} \tag{14}$$

Once the length a is known, the induced velocity components at any point (ζ, r) are obtained as follows:

$$\frac{u(\zeta, r)}{V} = \frac{(\zeta_o^2 - a^2)^2}{4\zeta_o a} \left\{ \frac{(\zeta + a)}{\left[(\zeta + a)^2 + r^2\right]^{3/2}} - \frac{(\zeta - a)}{\left[(\zeta - a)^2 + r^2\right]^{3/2}} \right\} \tag{15}$$

$$\frac{v(\zeta, r)}{V} = \frac{(\zeta_o^2 - a^2)^2}{4\zeta_o a} \left\{ \frac{r}{\left[(\zeta + a)^2 + r^2\right]^{3/2}} - \frac{r}{\left[(\zeta - a)^2 + r^2\right]^{3/2}} \right\} \tag{16}$$

The body shape for the Rankine body is determined in nondimensional form only by the fineness ratio. The shape is obtained by finding those values of the two coordinates ζ and r (or θ_1, θ_2, and r) that cause the stream function to be zero, or

$$\psi = r^2 + \frac{(\zeta_o^2 - a^2)^2}{2a\zeta_o} (\cos \theta_2 - \cos \theta_1) = 0 \tag{17}$$

where θ_1 and θ_2 are defined in the preceding sketch.

Line Source-Point Sink Model

The case of a three-dimensional line source-point sink was examined, as shown in the sketch below.
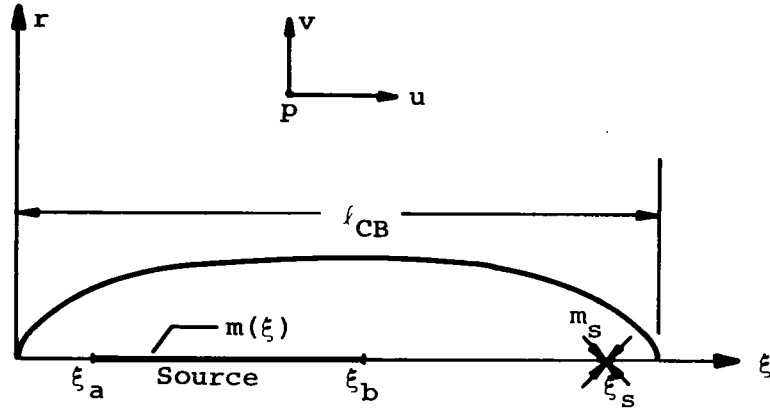
The stream function at a field point (ξ_p, r_p) due to the line source is

$$\psi_p = -\frac{1}{4\pi}\int_{\xi_a}^{\xi_b} m(\xi)\left[1 + \frac{\xi_p - \xi}{\sqrt{(\xi_p - \xi)^2 + r_p^2}}\right]d\xi \qquad (18)$$

and the axial velocity component is

$$u_p = \frac{1}{4\pi}\int_{\xi_a}^{\xi_b}\frac{m(\xi)(\xi_p - \xi)}{\left[(\xi_p - \xi)^2 + r_p^2\right]^{3/2}}d\xi \qquad (19)$$

The source strength distribution was assumed to have the following form

$$\frac{m}{4\pi\ell_{CB}V} = M_0 + M_1\xi' + M_2\xi'^2 + M_3\xi'^3 \qquad (20)$$

where the prime denotes nondimensionalization by ℓ_{CB}. Equation (20) can be put into equations (18) and (19), which are then integrated to obtain the following expressions:

$$-\left.\frac{\psi_p}{\ell_{CB}V}\right|_{source} = M_0\left[\xi_b' - \xi_a' + \xi_p'G_0 - G_1\right] + M_1\left[\frac{\xi_b'^2 - \xi_a'^2}{2} + \xi_p'G_1 - G_2\right]$$

$$+ M_2\left[\frac{\xi_b'^3 - \xi_a'^3}{3} + \xi_p'G_2 - G_3\right] + M_3\left[\frac{\xi_b'^4 - \xi_a'^4}{4} + \xi_p'G_3 - G_4\right] \tag{21}$$

and

$$\left.\frac{u}{V}\right|_{source} = \xi_p'\left[M_0 I_0 + M_1 I_1 + M_2 I_2 + M_3 I_3\right]$$

$$- \left[M_0 I_1 + M_1 I_2 + M_2 I_3 + M_3 I_4\right] \tag{22}$$

where the G_n are integrals of the form

$$G_n = \int_{\xi_a'}^{\xi_b'} \frac{(\xi')^n}{\sqrt{(\xi_p' - \xi')^2 + r_p'^2}}\, d\xi' \tag{23}$$

and the I_n are integrals of the form

$$I_n = \int_{\xi_a'}^{\xi_b'} \frac{(\xi')^n}{\left[(\xi_p' - \xi')^2 + r_p'^2\right]^{3/2}}\, d\xi' \tag{24}$$

The sink at ξ_s has a strength m_s equal to the negative of the integral of the source strength per unit length over its length. The sink then has a stream function value at p given by

$$\left.\frac{\psi}{\ell_{CB}^2 V}\right|_{sink} = \left[1 + \frac{\xi_p' - \xi_s'}{\sqrt{(\xi_p' - \xi_s')^2 + r_p'^2}}\right]\left[M_0(\xi_b' - \xi_a') + \frac{M_1}{2}(\xi_b'^2 - \xi_a'^2)\right.$$

$$\left. + \frac{M_3}{3}(\xi_b'^3 - \xi_a'^3) + \frac{M_4}{4}(\xi_b'^4 - \xi_a'^4)\right] \tag{25}$$

21

and an axial velocity given by

$$\left.\frac{u}{V}\right|_{sink} = \left\{\frac{\xi'_p - \xi'_s}{\left[(\xi'_p - \xi'_s)^2 + r'^2_p\right]^{3/2}}\right\}\left[M_o(\xi'_b - \xi'_a) + \frac{M_1}{2}(\xi'^2_b - \xi'^2_a)\right.$$

$$\left. + \frac{M_3}{3}(\xi'^3_b - \xi'^3_a) + \frac{M_4}{4}(\xi'^4_b - \xi'^4_a)\right] \tag{26}$$

The contributions of the free stream to the stream function and axial velocity at the point (ξ'_p, r'_p) are

$$\left.\frac{\psi}{\ell_{CB}{}^2 V}\right|_V = \frac{1}{2}r'^2_p \tag{27}$$

$$\left.\frac{u}{V}\right|_V = 1 \tag{28}$$

In order to obtain values for the four unknown source coefficients in equation (20), one condition on velocity and three conditions on stream function are used. The velocity condition is that $u/V = 0$ at the forward stagnation point. Equations (22), (26), and (28) are used. The stream function on the body contour is zero. Thus, the stream functions due to the source, sink, and free stream, equations (21), (25), and (27), are combined and set equal to zero for three selected points on the centerbody surface. Upon calculation of the source coefficients, the body shape can be located by computing values of ψ at various r'_p for a given value of ξ'_p until the $\psi = 0$ line is obtained.

Point Source Model

The last three-dimensional approach involves using discrete sources distributed in a predetermined manner along the centerbody axis. The axial and radial velocities induced by the sources plus the free stream were summed and their vector direction set equal to the slope of the centerbody surface at a sufficient number of points that the unknown source strengths could be computed. The condition was also invoked that the net source strength be zero to obtain a closed body. The body shape was then obtained by finding the $\psi = 0$ line as before.

A computer program was written to perform the calculation. The spacing of the sources was varied, and it was found that a spacing which is proportional to the local surface ordinate worked best. Thus, the sources are concentrated towards the ends of the body. This approach was successful in obtaining smooth, accurate body shapes; however, a number of trials were necessary. A relatively large number of points were required and, of course, the requirement that body slopes rather than ordinates be known is a disadvantage to the method.

Comparison of Models

Most ducted fan centerbodies are relatively blunt at the nose, in which case the Rankine body would be expected to give reasonable results for induced velocities for large as well as small centerbodies. The centerbody on the Bell X-22A ducted propeller (ref. 18) is rather slender, however, and provides a severe test for the Rankine body model. Of the comparisons made with the various centerbody models, two sets of results are shown to illustrate the nature of the results. The first set is for the Bell centerbody and the second is for the blunter centerbody used in the Doak VZ-4DA ducted fan (ref. 19). In these comparisons, the fit to the actual body and induced velocities at the fan station are shown. The former is of interest because a good fit is an indication of the accuracy of the computed induced velocities.

The slender-body line source results for the Bell X-22A centerbody are shown in figure 3(a). The body is made up of the nose shape which is determined by a line source and an aft portion determined by a point sink. The calculated shape of each portion is independent of the other portion; thus, the body is made up of two separate curves shown as dashed lines. Since the integrated source strength is equal to the sink strength, both the nose fit and the aft end fit represent the "nose" shapes of semi-infinite bodies having the same asymptotic radius. The computed nose of the body is slightly irregular, but it is generally a good fit to the actual body. However, the quality of the fit is dependent on the choice of body points and the length of the line source, and several attempts were necessary to obtain the fit shown.

The Rankine body approximation to the same centerbody is shown in figure 3(b), where the Rankine body is determined by the maximum

centerbody radius and its axial location. This approach results in a calculated centerbody model which is larger than the actual body. Although not shown, a Rankine body was also determined using the centerbody radius at the propeller and its axial location. Even though the latter centerbody was much smaller than the former, the axial velocities induced by both Rankine bodies in the plane of the propeller differed by only a small amount.

The third approximation to the Bell centerbody is obtained from the three-dimensional line source-point sink method and is shown in figure 3(c). The nose of the body is fit very well, but the results at the aft end of the body are poor. It was found that the choice of body points and the length and position of the line source were very critical in determining a good fit to the actual body. Many combinations of the above parameters were tried before the shape in figure 3(c) was obtained, and this result is obviously not optimum.

The last approach to approximating the Bell centerbody is the three-dimensional distribution of discrete point sources. The resulting fit is shown in figure 3(d). This method gives the best fit to the centerbody shape, but it has the previously discussed disadvantage of requiring knowledge of the body slopes at a large number of points. Also, several attempts were necessary to find the locations of the sources which would give a good fit to the body.

The axial velocities induced in the propeller plane by all four centerbody models are compared in figure 3(e). As expected from examining the body shapes, the Rankine body induces the largest axial velocity. The velocities induced by the slender-body line source and point source models are in good agreement. Since the inflow to the propeller is typically twice the free-stream velocity, the maximum centerbody contribution is only about 5 percent of the total inflow. Thus, the differences illustrated in figure 3(e) are not significant. The differences in axial velocity shown in figure 3(e) at $r/R_p = 1.0$ are indicative of the differences between the models in velocities induced along the duct reference cylinder. Although the differences shown are as high as 50 percent, the velocities at the reference cylinder are less than 1 percent of the free-stream velocity, and consequently have a negligible effect on duct loading. The importance of the

centerbody-induced effects on the X-22A ducted propeller were also substantiated by calculations made with and without a Rankine centerbody, which illustrated a negligible effect of the centerbody on forces and moments. Thus, the Rankine body model appears satisfactory for small, slender centerbodies (say, $R_{CB}/R_p < 0.30$).

Three of the four centerbody models were applied to the blunt centerbody used on the Doak VZ-4DA ducted fan (ref. 19). The results obtained from the slender-body line source and the Rankine body models are presented in figure 4(a) and (b), respectively. The slender-body line source model does not work well for a long blunt-nosed centerbody, as the predicted shape, shown in figure 4(a), has a tendency to be rough. The Rankine body fits the nose of the Doak centerbody very well as shown in figure 4(b). The Rankine body shown is shorter than the actual centerbody, but it could be made longer without compromising the good fit at the nose.

The three-dimensional line source-point sink technique was applied to this centerbody, but the right combination of body points and line source length could not be chosen to give a good body fit. Thus, the results are not shown. The nose could be fit with some accuracy, but the remainder of the body was usually so erratic that the induced velocities were not reliable.

The axial velocities induced in the plane of the fan by the slender-body line source model and the Rankine body are compared in figure 4(c). The agreement between the two methods is reasonably good.

Based on the work done with the centerbody models and the comparisons illustrated, the following observations can be made. The two line-source models cannot be depended upon to consistently give reasonable shape fit results, particularly for blunt shapes. The difficulty may lie in the use of a power series for the source strength distribution, and perhaps the use of another form, such as a Fourier series, would improve results. In any case, a number of free parameters are involved in the fit and more than one trial would generally be required to obtain a satisfactory shape. The distributed sources model gives an accurate fit to any reasonable body shape, but has the disadvantage noted above of having a number of free parameters, which would require trial calculations. In addition, body slopes at a large number of axial stations are required, which adds

considerably to the task of preparing input data. The Rankine body fits blunted centerbodies reasonably well and has the advantage of no necessity for trial calculations because of the limited number of parameters.

ANGLE OF ATTACK CONSIDERATIONS

Although considerable work has been done in predicting ducted fan performance at angle of attack (refs. 3 and 6), this work was not incorporated into the computer program of reference 8. Thus, a part of the present investigation was directed towards some additional analysis on angle of attack effects and incorporation of the results into the computer program.

Method of Approach

The method of approach makes use of the capability of potential flow solutions to be superimposed. The first solution consists of the duct and fan operating in a uniform flow at zero angle of attack with velocity, $\overline{V}$, where

$$\overline{V} = V \cos \alpha \tag{29}$$

An equivalent advance ratio, $\overline{J}$ is used to compute ducted fan performance in axial flow, where

$$\overline{J} = J \cos \alpha \tag{30}$$

The fan and duct vorticities are then considered to be unchanged by the addition of the crossflow, $V \sin \alpha$. The thrust coefficients, however, are referenced to the true free-stream velocity.

The second solution is that for the duct at angle of attack. The duct at angle of attack is in a crossflow, $V \sin \alpha$, which must be cancelled at the duct surface. This is done by adding vorticity to the duct as described by Weissinger (ref. 20) for a ring wing at angle of attack. The vorticity consists of bound vortex rings which have a variation of strength around their circumference and trailing (free) vortex filaments caused by the circumferential strength variation of the rings. The strength variation of the non-axisymmetric bound vorticity is defined as

26

$$\gamma_\alpha = V \sin \alpha \cos \phi \left[c_o \cot \frac{\theta}{2} + \sum_{n=1}^{5} c_n \sin n\theta \right] \qquad (31)$$

from equation (4.2) of reference 20. This vorticity induces a radial velocity at the duct surface which exactly cancels the radial components of $V \sin \alpha$ and the velocity induced by the trailing non-axisymmetric vorticity associated with γ_α. Through the equation expressing the cancellation of the angle of attack-induced velocities at the duct surface, the c_n coefficients in equation (31) are determined. These coefficients are a function only of c/D and are tabulated in reference 20.

A vorticity of the form of equation (31) induces a non-axisymmetric, axial velocity distribution at the fan station. Some consideration was given to incorporating this effect into the fan loading and wake representation in reference 7. The resulting variable-strength, helical vortex pattern that occurs in the fan wake greatly complicates the analysis, and its inclusion was not considered justified. Thus, the angle of attack effects in the second solution were not considered to affect the velocities and loadings of the first (axisymmetric) solution. The forces and moments and pressure distribution include all effects, however.

Force and Moment Coefficients

The force distribution on the duct is obtained from a Lagally type of formulation for the action of one singularity upon another. According to this general approach, the velocities induced on a bound singularity by the free stream and trailing (free) singularity distribution produce a net force, whereas velocities induced on two bound singularities by each other cause equal and opposite forces and zero net force. In the latter case, however, a non-zero moment may be produced, even though the forces cancel.

A force is produced by a velocity acting on an element of vorticity. The force direction is normal to the plane formed by the velocity and vorticity vectors and is given by the right-hand rule. The following sign conventions are used in determining the forces acting on the duct. A positive vortex ring is one which adds axial velocity inside the duct. A positive radial velocity is radially outward from the centerline of the

duct, and a positive axial velocity is in the positive x-direction. The force and moment sign conventions are shown in figure 1.

Thrust.- A thrust force is obtained when an axisymmetric radial velocity acts on an axisymmetric vorticity and a non-axisymmetric radial velocity acts on a non-axisymmetric vorticity. Any other combination of velocity and vorticity in our formulation will result in a zero thrust force. Thus, the thrust on the duct is made up of the induced velocities v_γ, v_{γ_w}, and v_{CB} acting on γ_D, the crossflow velocity $-V \sin \alpha \cos \phi$ acting on γ_α, and the induced velocity v_{γ_t} acting on γ_α.

A radial velocity, v, acting on an element of vorticity, γ, results in a thrust per unit length

$$\frac{dT}{dx} = \int_0^{2\pi} \rho v \gamma R \, d\phi \tag{32}$$

Equation (32) can then be integrated over the chord of the duct to give the total thrust.

The first contribution to the thrust mentioned above is due to axisymmetric radial velocities acting on the axisymmetric vorticity γ_D. The induced velocities are

$$\frac{v_\gamma + v_{\gamma_w} + v_{CB}}{\overline{V}} = \sum_{n=0}^{5} \left(\frac{\gamma}{\overline{V}} B_n + A_n + D_n \right) \cos n\theta$$

$$\equiv \sum_{n=0}^{5} E_n \cos n\theta \tag{33}$$

using equations (8), (10), and (12) of reference 1. When equation (33) and equation (17) of reference 6 (which is also given as eq. (64)) are used in equation (32), there results

$$T_{D_1} = -\frac{\pi}{2} \rho c D \overline{V} \gamma \int_0^{\pi} \left(\sum_{n=0}^{5} E_n \cos n\theta \right) \left[C_o \cot \frac{\theta}{2} \right.$$

$$\left. + \sum_{m=1}^{5} C_m \sin m\theta \right] \sin \theta \, d\theta \qquad (34)$$

Defining a thrust coefficient as

$$C_{T_{D_1}} = \frac{T_{D_1}}{\frac{1}{2} \rho V^2 A} \qquad (35)$$

we get

$$C_{T_{D_1}} = -\pi \frac{c}{D} \frac{\gamma}{\overline{V}} \cos^2 \alpha \left[C_o (4E_o + 2E_1) + 2C_1 E_o \right.$$

$$\left. + \sum_{n=1}^{4} (C_{n+1} E_n - C_n E_{n+1}) \right] \qquad (36)$$

The second thrust component is obtained from equation (32) by expressing the radial velocity due to the crossflow as

$$v = -V \sin \alpha \cos \phi \qquad (37)$$

and using the vorticity γ_α from equation (31).

Equation (32) then gives the thrust on the γ_α vortex ring distribution as

$$\frac{dT_{D_2}}{dx} = \frac{\pi}{2} \rho D (V \sin \alpha) \left[c_o \cot \frac{\theta}{2} + \sum_{n=1}^{5} c_n \sin n\theta \right] \qquad (38)$$

Integrating equation (38) over the duct chord and using equation (35) we get

$$C_{T_{D_2}} = \pi \frac{c}{D} (2c_o + c_1) \sin^2 \alpha \qquad (39)$$

There is a second component of thrust on the γ_α vortex ring distribution due to the radial velocity induced by the trailing vortex filaments associated with γ_α acting on γ_α. The radial velocity distribution is computed using equation (1.4) of reference 21. After Fourier analysis, the distribution is written as

$$v_{\gamma_t} = V \sin \alpha \cos \phi \sum_{n=0}^{5} H_n \cos n\theta \tag{40}$$

Application of the same method used to develop equation (39) results in the following thrust coefficient.

$$C_{T_{D_3}} = - \frac{\pi}{2} \frac{c}{D} \sin^2 \alpha \left[c_0 (4H_0 + 2H_1) + 2c_1 H_0 \right.$$

$$\left. + \sum_{n=1}^{4} (c_{n+1} H_n - c_n H_{n+1}) \right] \tag{41}$$

The duct thrust due to the fan pressure jump acting on the duct surface aft of the fan is given by equation (25) of reference 1 as

$$C_{T_{D_4}} = \left[1 - \left(\frac{R_p}{R} \right)^2 \right] \frac{\Delta p_z}{\frac{1}{2} \rho \overline{V}^2} \cos^2 \alpha \tag{42}$$

The propeller thrust is given by equation (22) of reference 1 as

$$C_{T_P} = \frac{A_p}{A} \frac{N}{\pi z \overline{J}'} \sum_{n=1}^{z} \frac{\Gamma_n}{R\overline{V}} \cos^2 \alpha \tag{43}$$

In general, some axial force will exist on the centerbody, particularly if the flow over the aft part is separated. However, with a closed centerbody source-sink representation, there would be zero axial force in uniform flow (D'Alembert's paradox). To the extent that the axial velocity induced over the centerbody varies with x, there would be a small axial force, but this will be neglected.

30

The total thrust on the ducted fan is given by the sum of equations (36), (39), (41), (42), and (43).

Normal force.- An element of vorticity, γ, acted on by an axial velocity, u, results in an element of normal force

$$dN = \rho u \gamma R \cos \phi \, d\phi \qquad (44)$$

A net normal force will result on the duct only if an axisymmetric axial velocity acts on a non-axisymmetric vorticity or vice versa.

The first component of normal force is a result of the axial velocities u_{γ_D}, u_γ, u_{γ_w}, and u_{CB} acting on γ_α. The total induced axial velocity can be written as

$$\frac{u_{\gamma_D} + u_\gamma + u_{\gamma_w} + u_{CB}}{\overline{V}} = \sum_{n=o}^{5} \left[\frac{\gamma}{\overline{V}} \left(F_n^* + B_n^* \right) + A_n^* + D_n^* \right] \cos n\theta$$

$$\equiv \sum_{n=o}^{5} E_n^* \cos n\theta \qquad (45)$$

using equations (32), (9), (11), and (13) of reference 1. Integrating equation (44) around the duct gives the normal force on one ring vortex as

$$\frac{dN_{D_1}}{dx} = \pi\rho V^2 R \sin\alpha \cos\alpha \left(\sum_{n=o}^{5} E_n^* \cos n\theta \right) \left(c_o \cot \frac{\theta}{2} \right.$$

$$\left. + \sum_{m=1}^{5} c_m \sin m\theta \right) \qquad (46)$$

Integrating equation (46) over the duct chord and defining normal-force coefficient to be

$$C_{N_{D_1}} = \frac{N_{D_1}}{\frac{1}{2} \rho V^2 A} \qquad (47)$$

31

we get

$$C_{N_{D_1}} = \frac{\pi}{2} \frac{c}{D} \sin \alpha \cos \alpha \left[c_o (4E_o^* + 2E_1^*) + 2c_1 E_o^* \right.$$

$$\left. + \sum_{n=1}^{4} (c_{n+1} E_n^* - c_n E_{n+1}^*) \right] \tag{48}$$

There is a normal force due to u_{γ_α} acting on γ_D. From equation (31) of reference 1,

$$\frac{u_{\gamma_\alpha}}{V} = \sin \alpha \cos \phi \sum_{n=o}^{5} G_n^* \cos n\theta \tag{49}$$

and from integration of equation (44) the normal force on one vortex ring is

$$\frac{dN_{D_2}}{dx} = \pi \rho V R \gamma \sin \alpha \left(\sum_{n=o}^{5} G_n^* \cos n\theta \right) \left(C_o \cot \frac{\theta}{2} \right.$$

$$\left. + \sum_{m=1}^{5} C_m \sin m\theta \right) \tag{50}$$

Using equation (47), the total component is

$$C_{N_{D_2}} = \frac{\pi}{2} \frac{c}{D} \frac{\gamma}{V} \sin \alpha \cos \alpha \left[C_o (4G_o^* + 2G_1^*) + 2C_1 G_o^* \right.$$

$$\left. + \sum_{n=1}^{4} (C_{n+1} G_n^* - C_n G_{n+1}^*) \right] \tag{51}$$

The free vortex filaments trailing from the γ_α vortex ring distribution do not induce an axial component of velocity. Thus, their contribution acting on the γ_D distribution is zero.

32

The normal-force coefficient resulting from the axial component of the free stream, V cos α, acting on γ_α is

$$C_{N_{D_3}} = \pi \frac{c}{D} (2c_o + c_1) \sin \alpha \cos \alpha \tag{52}$$

The fan sustains a normal force at angle of attack. Estimates of the size of this force were made in reference 2 on the basis of open propeller results, and the effect was found to be small compared to the duct normal force. In addition, the duct tends to align the flow with the fan axis. Consequently, the fan normal force contribution was neglected.

The centerbody can also sustain a normal force. Using slender-body theory as a guide, for a pointed-tail, centerbody-like shape with no flow separation, there will be a normal force distribution along the body length but zero net normal force. Viscous effects will cause some normal force to exist, but the net effect should be small, particularly since the duct tends to align the flow. Thus, the normal force on the centerbody was neglected. The total normal force on the ducted fan is given by the sum of equations (48), (51), and (52).

Pitching moment.- The pitching moment on the ducted fan is taken as positive if it tends to rotate the nose up. The center of moments is on the duct centerline at the midchord. Both normal force and thrust-type forces contribute to the total pitching moment. The normal force adds to the moment because it is distributed over the duct chord; therefore, a normal force, dN, acting at a distance x from the leading edge of the duct results in a moment

$$dM = dN \left(\frac{c}{2} - x \right) \tag{53}$$

The particular combinations of induced velocity and vorticity which produce a net thrust force do not produce a moment, but the thrust forces which cancel when considered over the entire duct do add a moment to the duct. Thus, a thrust force, dT, acting on the reference cylinder at an azimuth angle, ϕ, produces a moment

$$dM = dT(R)(\cos \phi) \tag{54}$$

We will now consider all the combinations of induced velocity and vorticity to determine the total pitching moment on the duct.

A moment results from the distribution of normal force due to u_{γ_α} acting on γ_D. The normal force given by equation (50) is substituted into equation (53). The total pitching moment is obtained by integrating over the duct chord. Thus

$$M_{D_1} = \frac{\pi}{4}\,\rho R c^2 \gamma V \sin\alpha \int_0^\pi \sin\theta\,\cos\theta \left(\sum_{n=0}^{5} G_n^* \cos n\theta \right) \left(c_0 \cot \frac{\theta}{2} \right.$$

$$\left. + \sum_{m=1}^{5} C_m \sin m\theta \right) d\theta \tag{55}$$

Defining the pitching-moment coefficient as

$$C_{M_{D_1}} = \frac{M_{D_1}}{qAR} \tag{56}$$

equation (55) becomes

$$C_{M_{D_1}} = \frac{\pi}{4}\left(\frac{c}{D}\right)^2 \frac{\gamma}{V} \sin\alpha\,\cos\alpha \left[C_0(4G_0^* + 4G_1^* + 2G_2^*) \right.$$

$$+ C_1(G_1^* - G_3^*) + C_2(2G_0^* - G_4^*)$$

$$\left. + C_3(G_1^* - G_5^*) + C_4 G_2^* + C_5 G_3^* \right] \tag{57}$$

A moment results from the axial component of the free stream, $V \cos\alpha$, acting on γ_α. The normal force distribution is given by

$$dN = 2\rho V^2 R \sin\alpha\,\cos\alpha \left(c_0 \cot \frac{\theta}{2} + \sum_{n=1}^{5} c_n \sin n\theta \right) \tag{58}$$

34

which when substituted into equation (53) and integrated over the duct chord gives the pitching moment coefficient contribution

$$C_{M_{D_2}} = \frac{\pi}{2} \left(\frac{c}{D}\right)^2 (2c_0 + c_2) \sin \alpha \cos \alpha \qquad (59)$$

The induced axial velocities u_{γ_D}, u_γ, u_{γ_w}, and u_{CB} acting on γ_α produce a normal force distribution given by equation (46). The resulting pitching moment is

$$C_{M_{D_3}} = \frac{\pi}{4} \left(\frac{c}{D}\right)^2 \sin \alpha \cos \alpha \left[c_0(4E_0^* + 4E_1^* + 2E_2^*) + c_1(E_1^* - E_3^*) \right.$$

$$\left. + c_2(2E_0^* - E_4^*) + c_3(E_1^* - E_5^*) + c_4 E_2^* + c_5 E_3^* \right] \qquad (60)$$

A moment also results from the non-axisymmetric axial forces caused by v_{γ_D}, v_γ, v_{γ_w}, and v_{CB} acting on γ_α. By analogy with equation (33), we will express the induced velocity as

$$\frac{v_{\gamma_D} + v_\gamma + v_{\gamma_w} + v_{CB}}{\overline{V}} = \sum_{n=0}^{5} \left[\frac{\gamma}{\overline{V}} (B_n + F_n) + A_n + D_n \right] \cos n\theta$$

$$\equiv \sum_{n=0}^{5} E_n' \cos n\theta \qquad (61)$$

The resulting pitching-moment coefficient is

$$C_{M_{D_4}} = -\frac{\pi}{2} \frac{c}{D} \sin \alpha \cos \alpha \left[c_0(4E_0' + 2E_1') + 2c_1 E_0' \right.$$

$$\left. + \sum_{n=1}^{4} (c_{n+1} E_n' - c_n E_{n+1}') \right] \qquad (62)$$

35

There are three components of pitching moment caused by γ_D to be considered. A moment due to non-axisymmetric axial forces is caused by the crossflow component of the free stream, $V \sin \alpha \cos \theta$, acting on γ_D. A similar moment results from v_{γ_α} also acting on γ_D. Still another moment is due to the radial velocity induced by the non-axisymmetric trailing vortex filaments associated with γ_α acting on γ_D. However, γ_α is the bound vorticity that induces a radial velocity that exactly cancels the free-stream crossflow velocity and the radial velocity induced by the trailing vortex filaments. Thus, the above three moments should exactly cancel one another.

The centerbody and fan are both sources of a pitching moment. On the basis of the results of reference 2, an open propeller produces a negative moment. The centerbody in a uniform crossflow would produce a positive moment, on the basis of a slender-body type loading. On the basis that the duct tends to align the flow, these moments were neglected. The total pitching moment on the ducted fan is given by the sum of equations (57), (59), (60), and (62).

DUCT SURFACE PRESSURE DISTRIBUTION

The duct surface pressure distribution is obtained by first predicting the bound vorticity and velocity distribution over the duct reference cylinder, then including the effect of duct thickness to obtain the surface velocity distribution, and finally using Bernoulli's law to get the duct surface pressure coefficient. The basic method is the same as described in reference 6.

The velocity distribution over the duct reference cylinder is given by

$$u = \pm \frac{\gamma_D}{2} \pm \frac{\gamma_\alpha}{2} + V \cos \alpha + u_\gamma + u_{\gamma_w} + u_{\gamma_D} + u_{CB} + u_{\gamma_\alpha} \qquad (63)$$

where the plus (+) sign refers to the inner surface of the duct and the minus (-) sign refers to the outer surface. When the surface velocity is considered at a point off the vertical plane of symmetry of the duct, there is a tangential component of the free stream, $V \sin \alpha \sin \phi$, which must be added vectorally to equation (63).

36

The components of equation (63) are computed in the following manner. The duct-bound vorticity, γ_D, is obtained from equation (17) of reference 6 as

$$\frac{\gamma_D}{\gamma} = C_o \cot \frac{\theta}{2} + \sum_{n=1}^{5} C_n \sin n\theta \tag{64}$$

and the bound vorticity associated with a ring wing at angle of attack, γ_α, is given by equation (31). $V \cos \alpha$ is the axial component of the free stream. The axial velocities, u_γ and u_{γ_w}, induced by the outer trailing vortex cylinder and the inner wake cylinders respectively, are computed using equation (20) of reference 5, which is based on the results of reference 22. The velocity, u_{γ_D}, induced by the duct-bound vorticity (γ_D) is computed using equation (A-9) of reference 7. An alternate equation for this velocity is equation (18) of reference 6. The velocity induced by the centerbody, u_{CB}, is obtained from equation (15). When the duct is at angle of attack, the velocity u_{γ_α} is computed using equation (49). Thus we have all the components of equation (63) which give the velocity induced on the reference cylinder of the duct. We assume that this velocity is the same as that induced on the duct camberline. Using two-dimensional airfoil theory as an analogy, this velocity must be corrected for duct thickness effects.

From two-dimensional airfoil theory, the continuous part of the velocity distribution on the camberline is $u/V = 1$. The continuous part of the surface velocity distribution with thickness (u_s/V) is given for various thickness airfoils in reference 16. We assume that the surface velocity on a two-dimensional airfoil is given by applying a correction factor, $F(x)$, to the camberline velocity. Thus the surface velocity is

$$\frac{u_s}{V} = F(x) \tag{65}$$

where $F(x)$ for NACA four-digit series airfoils is given for various thickness ratios in figure 5. By analogy, we shall obtain the continuous part of the duct surface velocity by multiplying the continuous part of the camberline velocity from equation (63) by $F(x)$ as follows.

37

$$\frac{u_s}{V} = \frac{u}{V} \times F(x) \qquad (66)$$

The bound vorticities γ_D and γ_α are singular at the leading edge of the duct ($\theta = 0$). In order to compute pressure distributions near the leading edge, the following approach is used. The chordwise distributions of bound vorticity in the form $\Delta v_a/V$ are listed in Appendix I of reference 16 for many airfoils. For the NACA four-digit series, it is evident that thickness has very little effect on the bound vorticity when $x/c > 0.1$ because $\Delta v_a/V$ is nearly equal to $\frac{1}{2\pi} \cot \frac{\theta}{2}$ as is shown in figure 6 for several thickness ratios. The γ_D and γ_α vorticities can be approximated near the leading edge ($x/c < 0.1$) by replacing $\cot \frac{\theta}{2}$ in equations (31) and (64) with the appropriate value from figure 6. When $x/c \geq 0.1$, there is no thickness effect and $\cot \frac{\theta}{2}$ can be computed with no numerical problems.

With the above corrections, the duct surface velocity becomes

$$\frac{u_s}{V} = \left[\cos \alpha + \frac{u_\gamma}{V} + \frac{u_{\gamma_w}}{V} + \frac{u_{\gamma_D}}{V} + \frac{u_{CB}}{V} + \frac{u_{\gamma_\alpha}}{V} \right] F(x) \pm \left(\frac{\gamma_D}{2} + \frac{\gamma_\alpha}{2} \right)_c \qquad (67)$$

where the subscript c on the last term indicates that the $\cot \frac{\theta}{2}$ terms are approximated only when $x/c < 0.1$ as described previously.

The duct surface pressure coefficient is obtained from Bernoulli's equation

$$c_p = 1 - \left(\frac{u_s}{V} \right)^2 \qquad (68)$$

using equation (67). On the inner duct surface downstream of the fan, the total pressure is increased by the pressure rise across the fan tip Δp_z, and c_p is increased by $\Delta p_z/q$.

CONCLUDING REMARKS

Analysis and programming work have been conducted to provide an improved capability to a computer program developed previously by the authors for predicting the performance of a ducted fan in a uniform

38

axial flow. Specifically, the capabilities have been added for modeling
the centerbody, providing nonlinear blade lift characteristics, calcu-
lating performance at very low advance ratios, computing duct surface
pressure distributions, and computing performance at angle of attack.
The computer program has been modified according to the results of this
work, and a user's manual has been prepared. Comparisons with data for
the Bell and Doak ducted propellers have been made, and the results have
been included in the user's manual (ref. 1) in order to indicate the
nature of the results to be expected from use of the program. The
comparisons are generally as favorable or better than those obtained
in reference 6, with the exception of pitching moment. Pitching moment
prediction is one area in which additional work would be most useful,
since the normal and thrust forces and duct pressure distributions seem
to be well predicted, at least for the low-pressure-ratio type of ducted
fan represented by the Bell and Doak units.

Present development in propulsion and propulsion/lift engines for
transport-type aircraft is causing these types of engines to resemble
essentially single-stage, high-pressure-ratio fans driven by an
airbreathing energy source within the centerbody. Historically, the
airframe manufacturer has been responsible for the exterior engine cowl,
or duct. The flow model described herein seems potentially well suited
to matching the basic engine to its external aerodynamic shape and
analyzing the total powerplant configuration. Thus, it seems logical
that an extension of the flow model reported herein be directed towards
the characteristics of the high-bypass-ratio turbofan or lift fan
engines. The two main areas that would need additional consideration
are the model of the high solidity, highly loaded fan stage and the
model of the centerbody consisting essentially of a turbojet engine
which accepts 1/5 to 1/10 of the inlet air but may produce up to half
of the total engine thrust.

Nielsen Engineering & Research, Inc.
        June 1969

REFERENCES

1. Mendenhall, M. R. and Spangler, S. B.:   A Computer Program for the Prediction of Ducted Fan Performance.   NASA CR 1495

2. Kriebel, A. R., Sacks, A. H., and Nielsen, J. N.:   Theoretical Investigation of Dynamic Stability Derivatives of Ducted Propellers. Vidya Rep. 63-95, Itek Corp., Jan. 9, 1963, AD 403 146.

3. Kriebel, A. R.:   Theoretical Investigation of Static Coefficients, Stability Derivatives, and Interference for Ducted Propellers. Vidya Rep. No. 112, Itek Corp., Mar. 31, 1964, AD 602 269 (published in part in Jour. of Aircraft, AIAA, vol. 1, no. 4, July-Aug. 1964).

4. Kriebel, A. R.:   Interference Between a Hull and a Stern-Mounted Ducted Propeller. Vidya Rep. No. 161, Itek Corp., Sept. 30, 1964, AD 612 019.

5. Kriebel, A. R. and Mendenhall, M. R.:   Interference Between a Hull and a Stern-Mounted Ducted Propeller. Vidya Rep. No. 204, Itek Corp., Oct. 30, 1965, AD 626 035.

6. Kriebel, A. R. and Mendenhall, M. R.:   Predicted and Measured Performance of Two Full-Scale Ducted Propellers. NASA CR 578, May 17, 1966.

7. Mendenhall, M. R., Kriebel, A. R., and Spangler, S. B.:   Theoretical Study of Ducted Propeller Blade Loading, Duct Stall and Interference. Vidya Rep. No. 229, Itek Corp., Sept. 1966, AD 646 022.

8. Mendenhall, M. R. and Spangler, S. B.:   Computer Programs for the Prediction of Ducted Propeller Performance. Vidya Rep. No. 230, Itek Corp., Sept. 1966.

9. Kaskel, A. L., Ordway, D. E., Hough, G. R., and Ritter, A.:   A Detailed Numerical Evaluation of Shroud Performance for Finite-Bladed Ducted Propellers. Therm, Inc., TAR-TR 639, Dec. 1963, AD 600 577.

10. Greenberg, M. D., Ordway, D. E., and Lo, C. F.:   A Three-Dimensional Theory for the Ducted Propeller at Angle of Attack. Therm Advanced Research, Inc., TAR-TR 6509, Dec. 1965, AD 480 994.

11. Morgan, W. B.:   Theory of the Annular Airfoil and Ducted Propeller. Fourth Symposium on Naval Hydrodynamics, Office of Naval Research, ACR-73, 1962.

12. Chaplin, H. R.:   A Method for Numerical Calculation of Slipstream Contraction of a Shrouded Impulse Disk in the Static Case with Application to Other Axisymmetric Potential Flow Problems. DTMB Rep. No. 1857, Jan. 1964, AD 604 127.

13. Caster, E. B.: A Computer Program for Use in Designing Ducted Propellers. Naval Ship Research and Development Center, Rep. 2507, Oct. 1967, AD 826 113.

14. Weissinger, J. and Maass, D.: Theory of the Ducted Propeller. A Review. Seventh Symposium on Naval Hydrodynamics, Rome, Italy, Aug. 25-30, 1968.

15. Morgan, W. B. and Caster, E. B.: Comparison of Theory and Experiment on Ducted Propellers. Seventh Symposium on Naval Hydrodynamics, Rome, Italy, Aug. 25-30, 1968.

16. Abbott, I. H. and von Doenhoff, A. E.: Theory of Wing Sections. Dover Publications, Inc., New York, N. Y., 1959.

17. Kuchemann, D. and Weber, J.: Aerodynamics of Propulsion. McGraw-Hill Book Co., Inc., New York, N. Y., 1953.

18. Mort, K. W. and Gamse, B.: A Wind-Tunnel Investigation of a 7-Foot-Diameter Ducted Propeller. NASA TN D-4142, Aug. 1967.

19. Mort, K. W. and Yaggy, P. F.: Aerodynamic Characteristics of a 4-Foot-Diameter Ducted Fan Mounted on the Tip of a Semispan Wing. NASA TN D-1301, Apr. 1962.

20. Weissinger, J.: On the Aerodynamics of Ring Wings. I. The Pressure Distribution on a Thin, Almost Axially Symmetric Wing in Subsonic Flow. Deutshen Versuchsanstalt Für Luftfahrt E. V. - Mülheim (Ruhr) Sept. 1955, translated by S. de los Santos, David Taylor Model Basin Aero. Rep. 899, June 1956, AD 102 118.

21. Weissinger, J.: Ring Airfoil Theory. Problems of Interference and Boundary Layer. Institute für Angewandte Mathematik der Technishen Hochshule Karsruhe, Jan. 1959, European Office ARDC, Contract No. AF 61(514)-1207, AFOSR TN 59-226, AD 211 809.
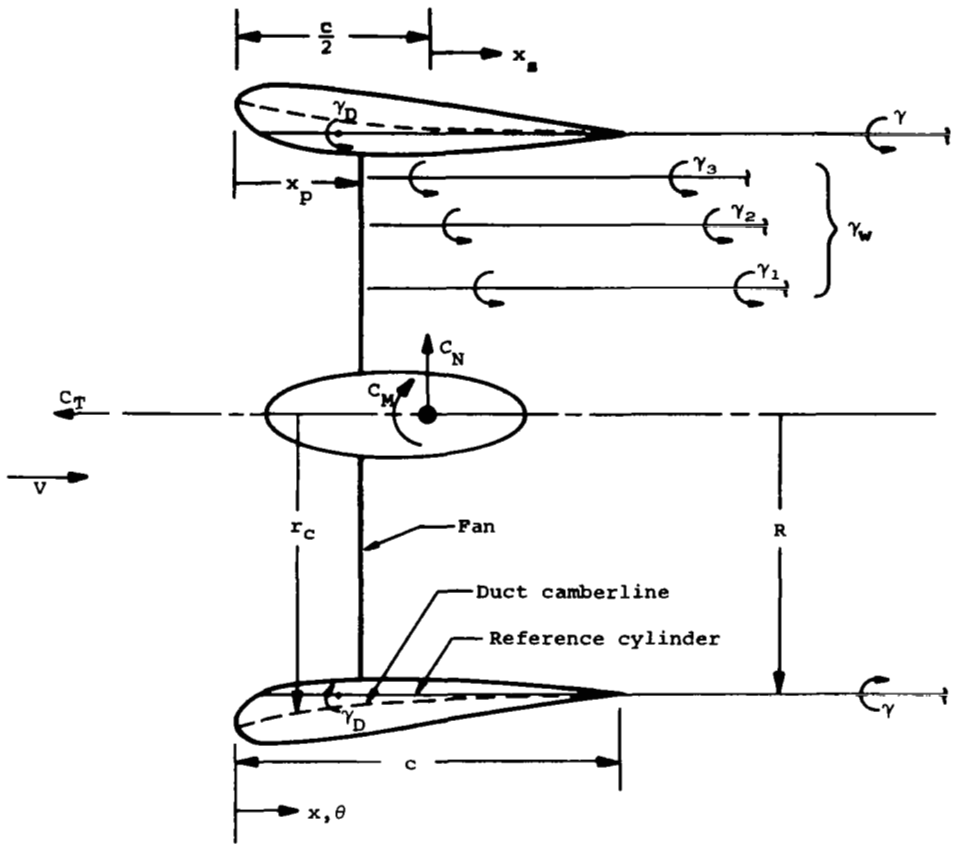
(a) Duct-fan-centerbody in axial flow.
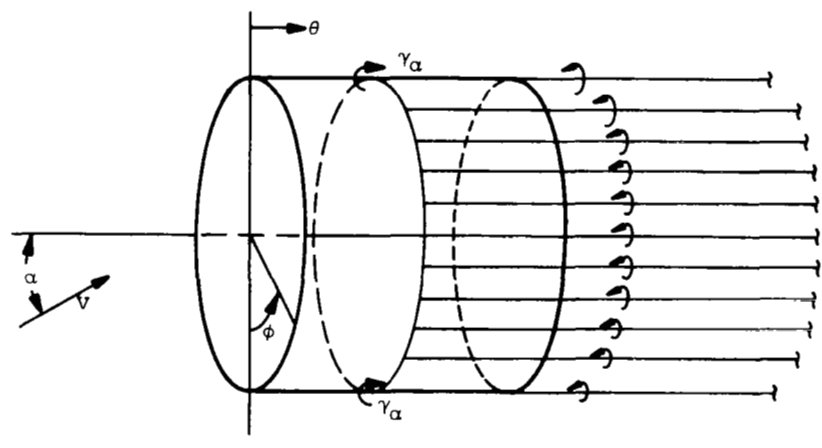
(b) Duct at angle of attack.

Figure 1.- Flow models for ducted fan.
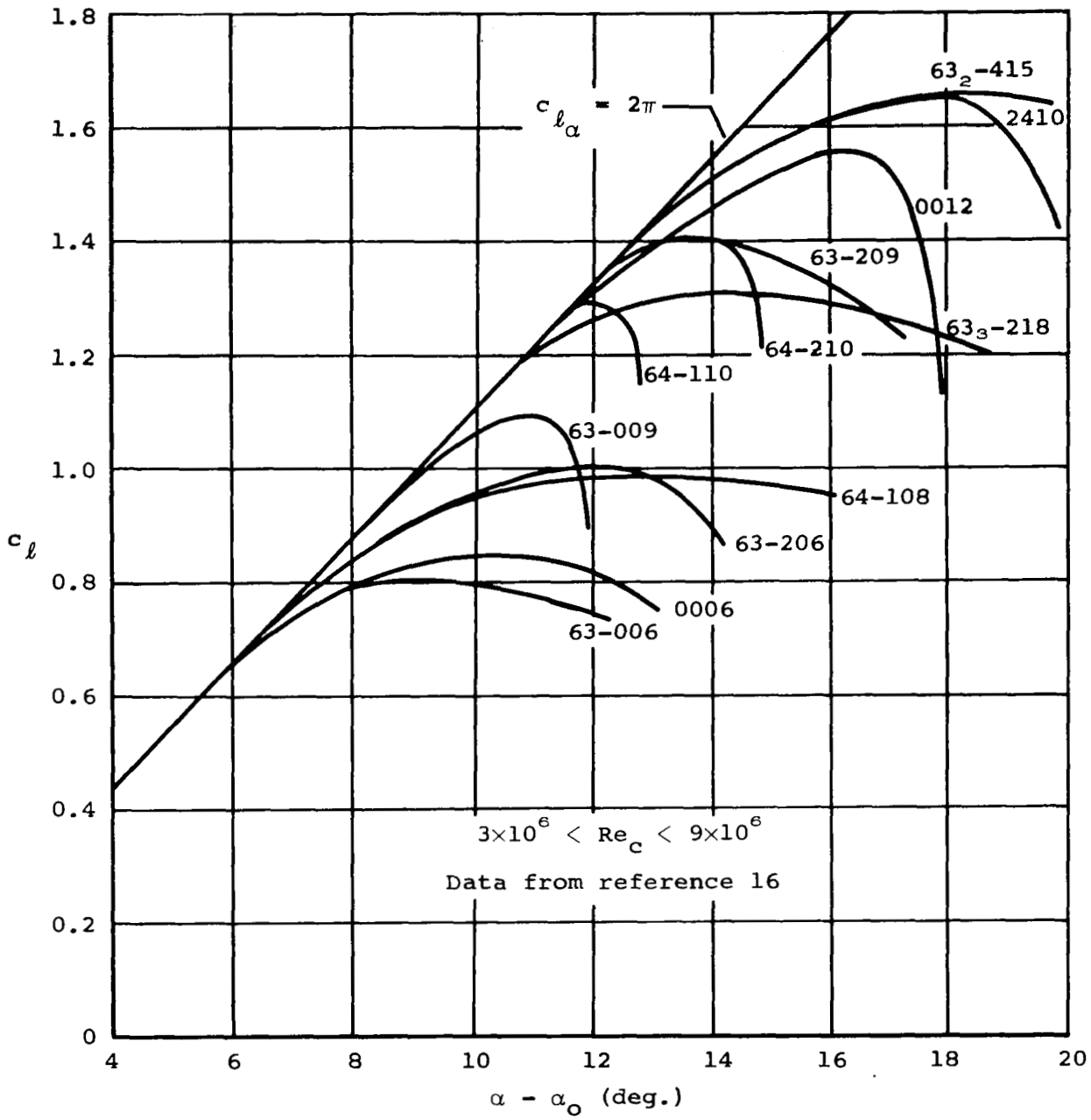
(a) Section data.

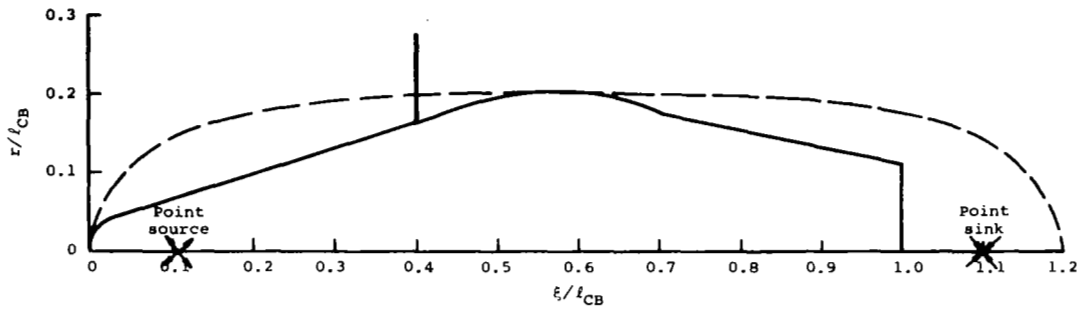Figure 2.- Airfoil section characteristics.

43
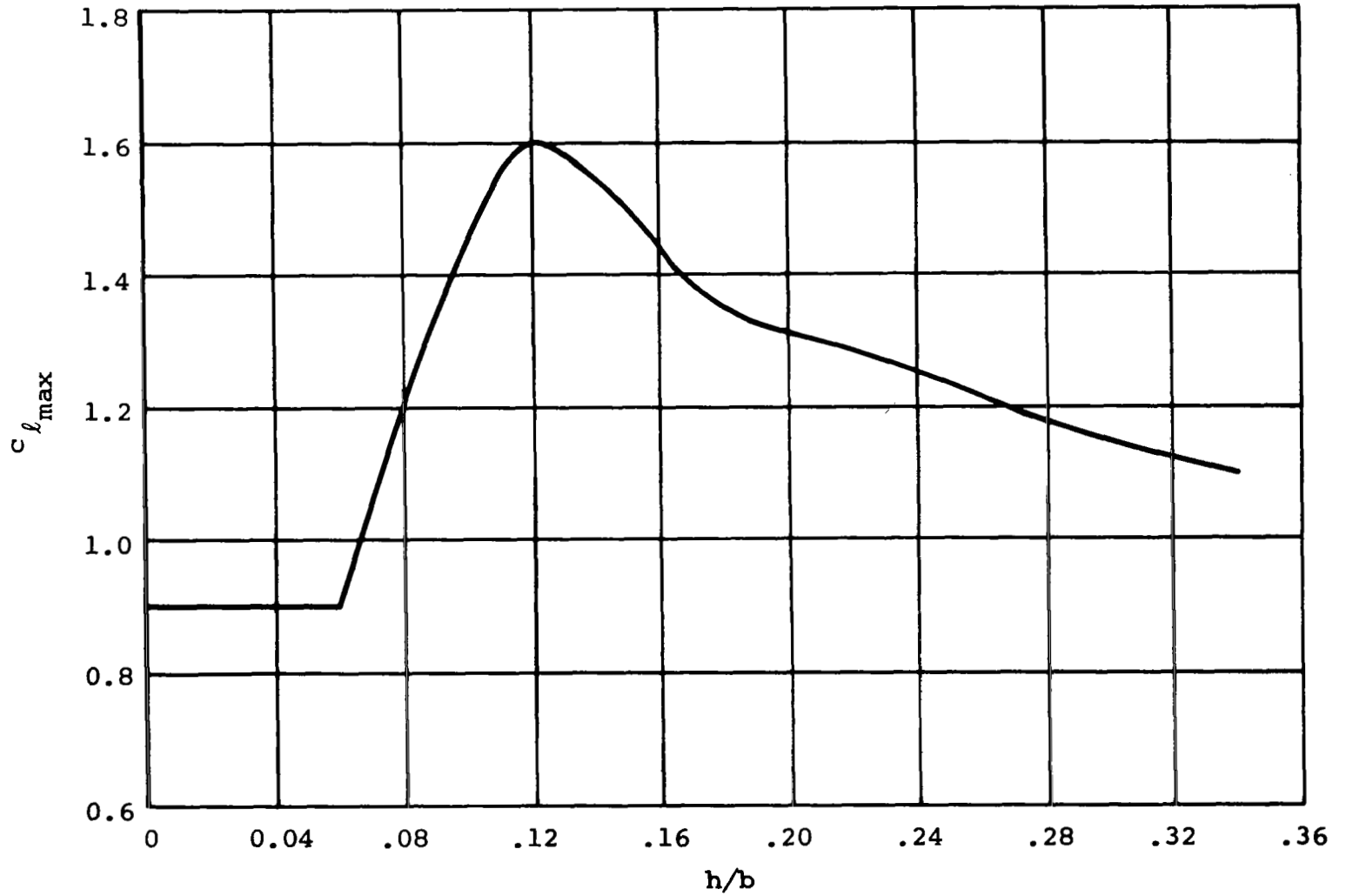
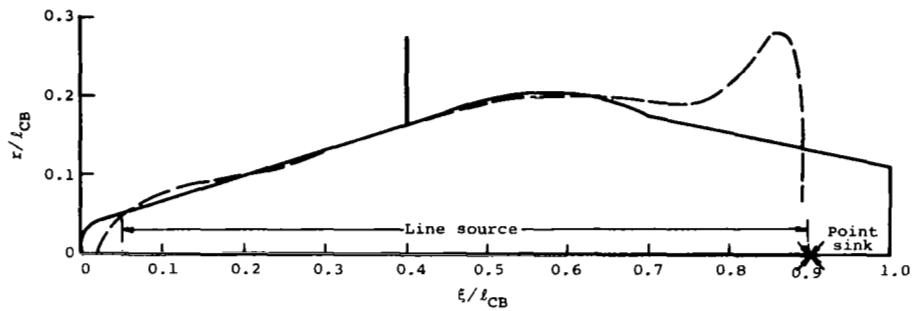(b) Assumed $c_{\ell_{max}}$ variation with blade thickness-to-chord ratio.
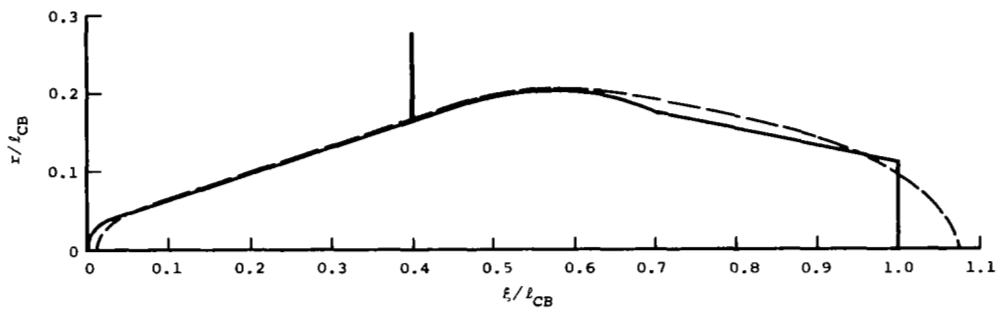
Figure 2.- Concluded.
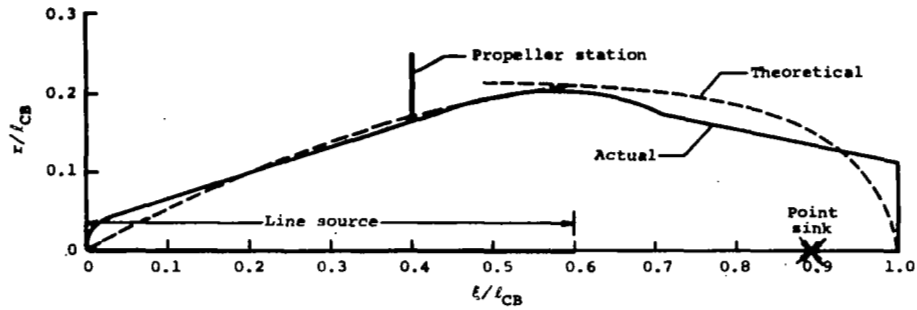
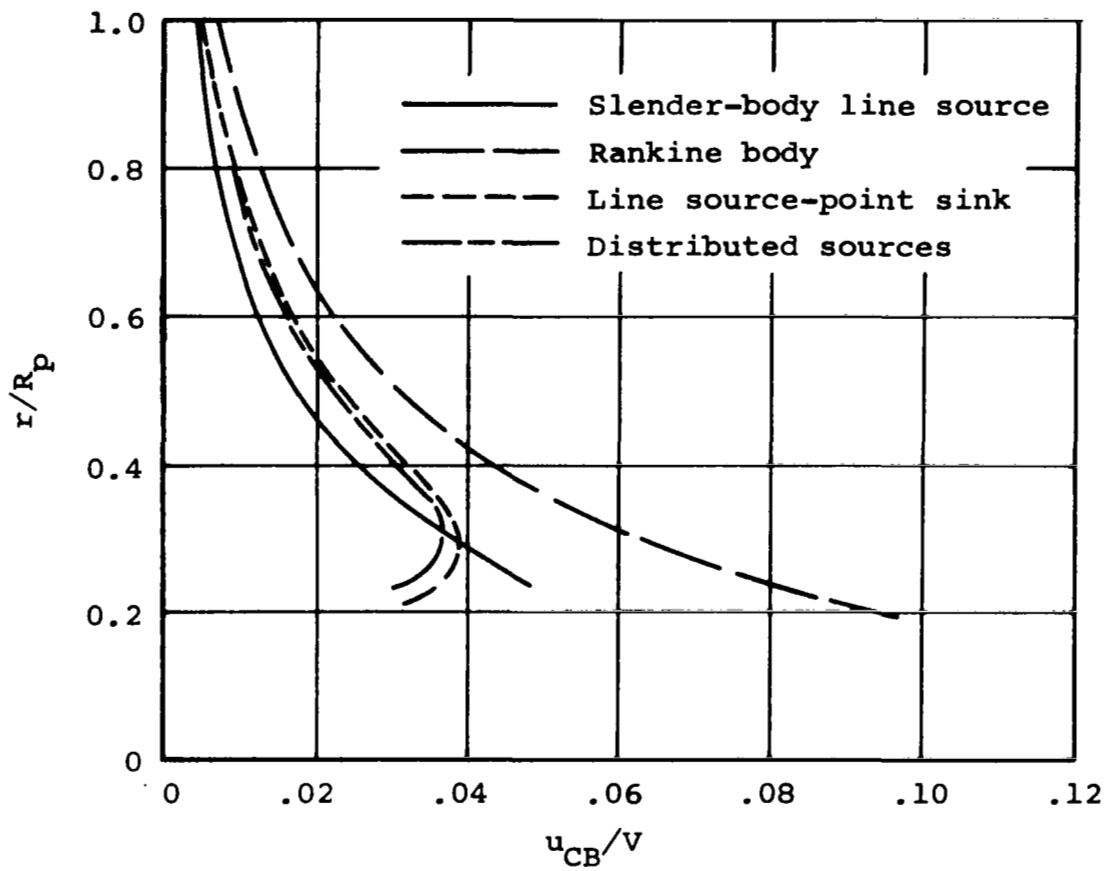(a) Slender-body line source with point sink.

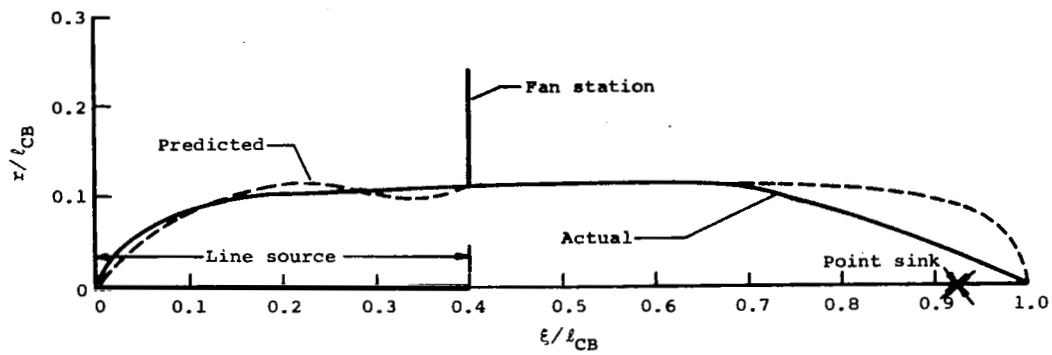(b) Rankine body.

(c) Three-dimensional line source-point sink.

(d) Three-dimensional distributed point sources.

Figure 3.- Comparison of centerbody models for the
Bell X-22A ducted propeller.

45

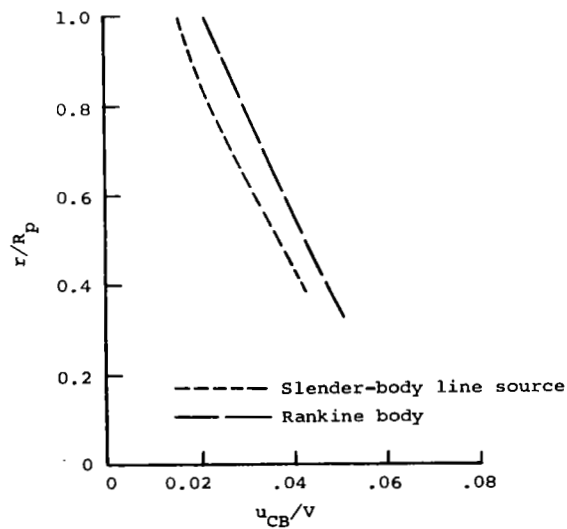(e) Centerbody-induced axial velocities at the propeller station.

Figure 3.- Concluded.

(a) Slender-body line source with point sink.
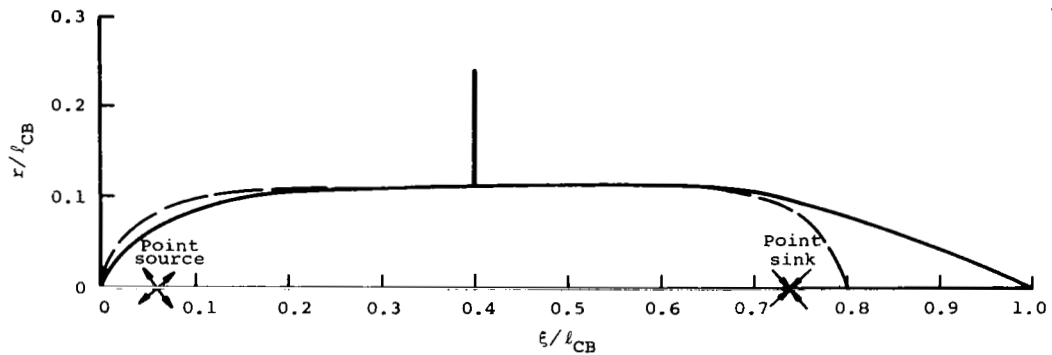
(b) Rankine body.

(c) Centerbody-induced axial velocities
at fan station.

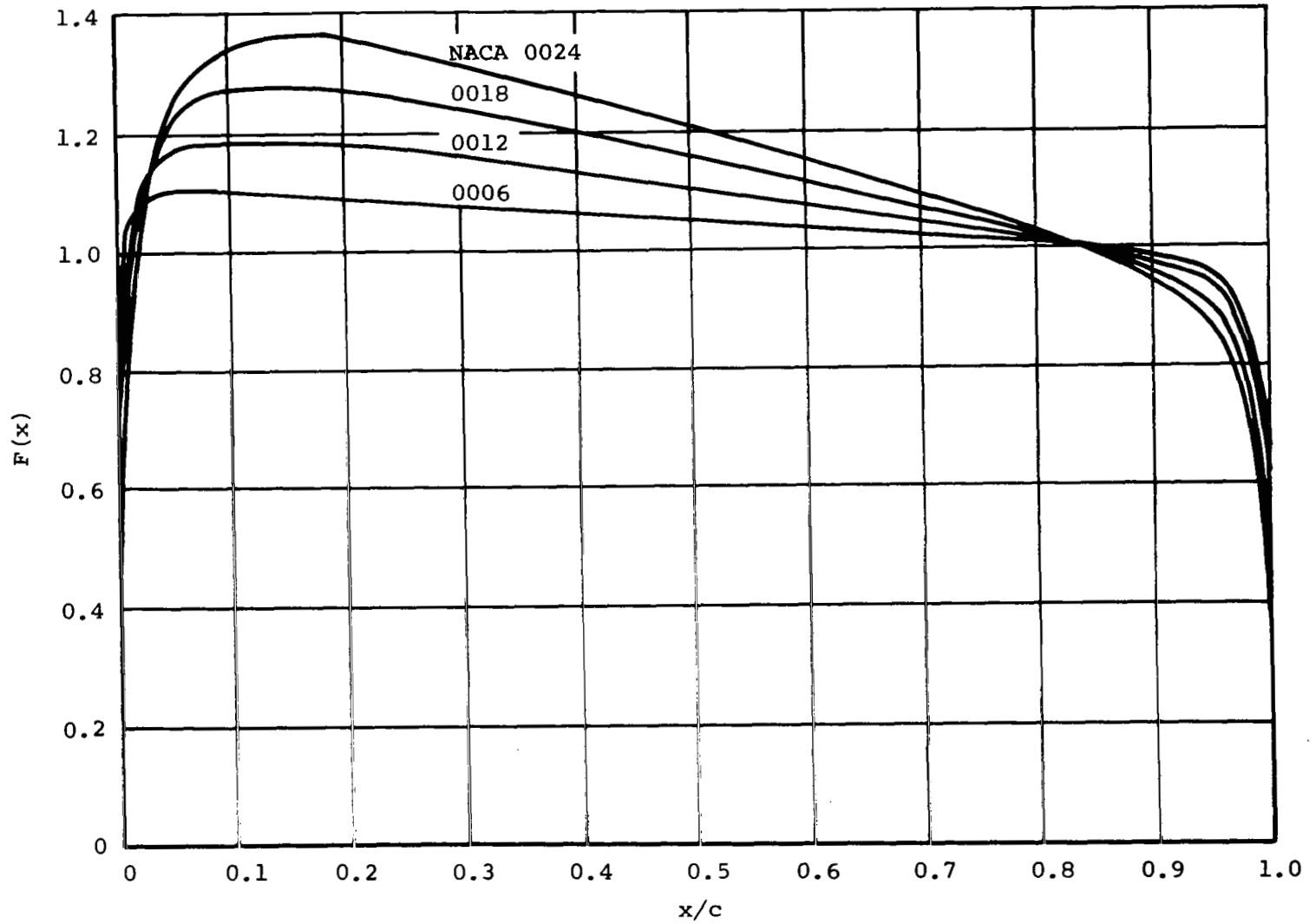Figure 4.- Comparison of centerbody models for the
Doak VZ-4DA ducted fan.

Figure 5.- Thickness correction factor for
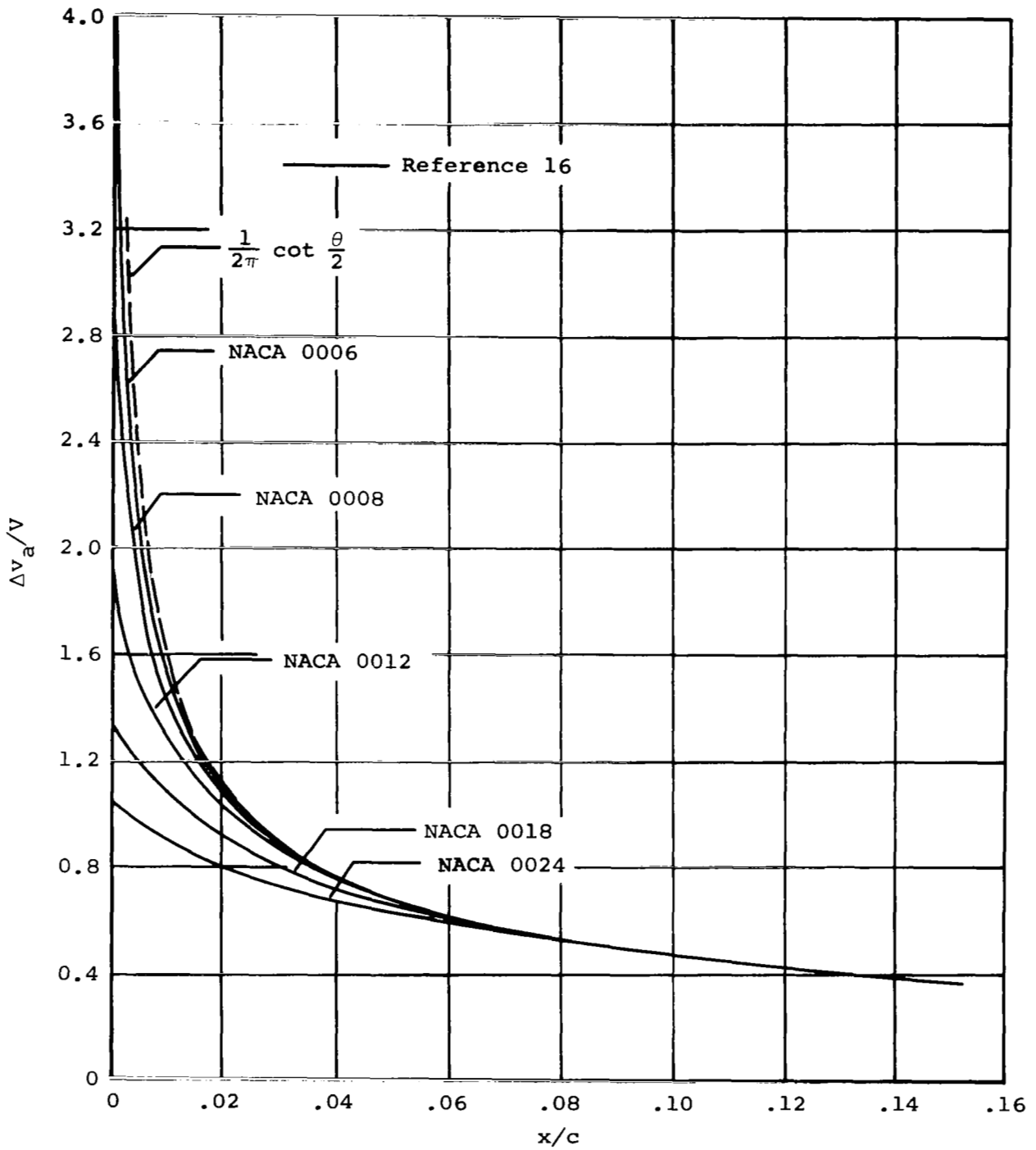surface velocity distributions.

Figure 6.- Bound vorticity distributions near the
leading edge of NACA four-digit series airfoils.